Received: 26 May 2023 | Revised: 25 December 2023 | Accepted: 12 May 2024

DOI: 10.1002/bit.28755

ARTICLE

BIOTECHNOLOGY AND BIOENGINEERING WILEY

In vitro degradation, swelling, and bioactivity performances of in situ forming injectable chitosan-matrixed hydrogels for bone regeneration and drug delivery

Fatma Zehra Kocak[1,2] | Muhammad Yar[3] | Ihtesham U. Rehman[4]

[1]Engineering-Architecture Faculty, Metallurgy and Materials Engineering, Nevsehir Haci Bektas Veli University, Nevsehir, Turkey

[2]Engineering Department, Lancaster University, Lancaster, UK

[3]Interdisciplinary Research Centre in Biomedical Materials (IRCBM), COMSATS University Islamabad, Lahore Campus, Lahore, Pakistan

[4]School of Medicine and Dentistry, University of Central Lancashire, Lancashire, UK

Correspondence

Fatma Zehra Kocak, Engineering-Architecture Faculty, Metallurgy and Materials Engineering, Nevsehir Haci Bektas Veli University, Nevsehir 50300, Turkey.
Email: fzkocak@nevsehir.edu.tr

Ihtesham U. Rehman, School of Medicine and Dentistry, University of Central Lancashire, Lancashire PR1 2HE, UK.
Email: iurehman@uclan.ac.uk

Funding information

Turkish Ministry of National Education

Abstract

Injectable, tissue mimetic, bioactive, and biodegradable hydrogels offer less invasive regeneration and repair of tissues. The monitoring swelling and in vitro degradation capacities of hydrogels are highly important for drug delivery and tissue regeneration processes. Bioactivity of bone tissue engineered constructs in terms of mineralized apatite formation capacity is also pivotal. We have previously reported in situ forming chitosan-based injectable hydrogels integrated with hydroxyapatite and heparin for bone regeneration, promoting angiogenesis. These hydrogels were functionalized by glycerol and pH to improve their mechano-structural properties. In the present study, functionalized hybrid hydrogels were investigated for their swelling, in vitro degradation, and bioactivity performances. Hydrogels have degraded gradually in phosphate-buffered saline (PBS) with and without lysozyme enzyme. The percentage weight loss of hydrogels and their morphological and chemical properties, and pH of media were analyzed. The swelling ratio of hydrogels (55%–68%(wt), 6 h of equilibrium) indicated a high degree of cross-linking, can be suitable for controlled drug release. Hydrogels have gradually degraded reaching to 60%–70% (wt%) in 42 days in the presence and absence of lysozyme, respectively. Simulated body fluid (SBF)-treated hydrogels containing hydroxyapatite-induced needle-like carbonated-apatite mineralization was further enhanced by heparin content significantly.

KEYWORDS

bioactivity, chitosan, degradation, heparin, hydroxyapatite, injectable hydrogel

1 | INTRODUCTION

The extracellular matrix (ECM) mimetic, porous and degradable naturally derived polymers functionalized with bioactive compounds as tissue engineered constructs offer a great potential in regenerative medicine. Integration of these unique properties with stimuli-responsive crosslinking mechanisms in situ at physiological conditions (e.g., pH and temperature) raise minimally invasive regenerative materials. Injectable hydrogels produced as fluid solution transform into cross-linked hydrogels in situ molding into tissue deficits for their

Abbreviations: ATR, attenuated total reflectance; CS, chitosan; DDA, degree of deacetylation; ECM, extracellular matrix; FT-IR, Fourier transform-infrared spectroscopy; GFs, growth factors; HA, hydroxyapatite; Hep, heparin; PBS, phosphate buffer saline; SBF, simulated body fluid; SEM, scanning electron microscopy.

reconstruction. Biodegradable hydrogels serve as temporary scaffolds stimulating healing ensured by the interaction of bioactive agents, integrated in hydrogel networks, with tissues.

Chitosan (CS) is a biocompatible and biodegradable natural polymer. CS is processed through deacetylation of chitin which is a natural polysaccharide. CS is composed of acetylated and deacetylated forms of glucosamine bond series at linear configurations (Jennings, 2017). CS possesses highly efficient in situ gelation capacity due to pH and/or temperature stimuli. The neutralizing CS with various gelling agents, such as β-glycerophosphate (β-GP) (Dessì et al., 2013), Na_2CO_3 (Li et al., 2014), and $NaHCO_3$ (Liu et al., 2011), leads physical crosslinking in situ at the vicinity of body temperature. The addition of $NaHCO_3$ into CS-β-GP hydrogels was reported to improve mechanical properties and biocompatibility (Deng et al., 2017).

The swelling and biodegradation features of CS can be controlled by adjusting its molecular weight (Mw) and degree of deacetylation (DDA) (Jennings, 2017). Tailoring these properties extends applications of CS toward tissue engineering applications from temporary regenerative and/or drug delivery tools to high lifespan devices (Do et al., 2022; Taghizadeh et al., 2022), for example, wound healing (Aleem et al., 2017; Lih et al., 2012; Shahzad et al., 2015, 2018), bone regeneration (Iqbal et al., 2017; Kocak et al., 2022a; Nájera-Romero et al., 2020; Qasim et al., 2015) and cartilage repair (Chenite et al., 2000; Hoemann et al., 2005; Méthot et al., 2016; Shive et al., 2006). The rate of biodegradation of tissue-engineered constructs must have a harmony with the normal tissue recovery process. CS is exposed to degradation mainly by either physical or chemical means. The swelling, fractures, and dissolution are considered among physical degradation ways. CS can be degraded chemically by hydrolytic degradation (with or without an enzyme), and by means of oxidation and depolymerization reactions. During hydrolysis of CS, glycosidic linkages are degraded at varying rates depending on Mw and crystallinity of CS, and the cross-linking degree in the case of CS-based hydrogels. CS can also expose to hydrolysis in the presence of enzymes in the human body, for example, lysozyme and chitinase. The secretion of lysozyme by phagocytic cells, such as macrophage and neutrophil at tissue defects, induces degradation of CS which breakdown into glucosamine and saccharide units leading to proteoglycans removed by metabolic activities in the body (Jennings, 2017).

The enriching natural polymers such as CS along with bioactive ceramics leads to construction of functional bone tissue scaffolds. Bioactivity plays a key role in the success of the tissue regeneration process. Bioactive scaffolds elicit specific physical and biochemical functionalities improving their integration with the interacted tissues. Some bioceramics, such as hydroxyapatite (HA) and its ionic substituted forms (AL-Hamoudi et al., 2022; Chaudhry et al., 2013; Juhasz & Best, 2012; Qasim, 2015), bioactive glasses, glass-ceramics, and glass ionomer cements (Juhasz & Best, 2012; Najeeb et al., 2016; Qasim, 2015), are prominent with their bioactivity. One of the most commonly used methods for testing bioactivity is measuring mineralization capacity in simulated body fluid (SBF). The incubation of bioactive ceramics in SBF leads to the formation of the carbonated apatite layer on their surface, anticipating their in vivo attachment performance with bone tissues (Kokubo & Takadama, 2006; Kong et al., 2006). HA and its biomimetic ionic substitutions exhibit potential bioactive features due to reactive anionic hydroxyl groups on its surface attracting biological molecules. It is reported that HA enhances osteointegration, osteoconductivity, and rapid induction of bone growth by improving cellular activities, for example, cell viability, cell and protein adhesion, and cell proliferation and differentiation (Arun Kumar et al., 2015; Kong et al., 2006). The mechanically brittle structure of HA is strengthened by forming composites with diverse natural or synthetic polymers to form bioactive and biodegradable scaffolds which is more effective for tissue regeneration (Sharma et al., 2021). HA integrated polymer- based bioactive composites in different forms, for example, coatings (Bedi et al., 2012; Darr et al., 2004; Kong et al., 2006), porous scaffolds (Dubnika & Zalite, 2014; Qasim, et al., 2015), and injectable materials (Chuysinuan et al., 2021; Kocak et al., 2020, 2022b; Sa et al., 2015) have been reported for bone repair and regeneration, and drug delivery applications. HA introduction into CS-based pH and thermosensitive hydrogels has been reported to enhance bioactivity, osteogenic differentiation, and gene expression of mesenchymal stem cells (Rogina et al., 2017). Furthermore, CS-HA hydrogels neutralized by $NaHCO_3$ at increased HA concentrations have been reported to indicate quick gelation, and their pre-osteoblast encapsulated forms inducing osteoinduction and increasing cell viability (Ressler et al., 2018).

In addition to surface bonding, structural bonding of biomaterials with tissues occurs by tissue growth towards the pores and interconnected channels forming a network for transit of nutrients and metabolic agents by blood through branched blood vessels. This brings out another aspect of bioactivity provided by development of proangiogenic tools leading to rapid neovascularization upon tissue destruction which is necessary for normal tissue healing process. The involvement of pre-vasculature developed through cell technologies is a strategy to promote angiogenesis (Rouwkema et al., 2006). Besides, the inclusion of proangiogenic, growth factor (GFs) in tissue engineering constructs has been reported (Amini et al., 2012). However, the forementioned technique involves the problems with cell origin and surgical challenges, and unconformity of pre-vasculatures with native blood vessels. The latter method also may lead to risks of toxicity and side effects due to a high dosage of GFs required for angiogenesis (Amini et al., 2012; Yancopoulos et al., 2000). Therefore, recent strategies investigate the use of natural biocompatible, biomimetic molecules, such as heparin (Hep) which is bioactive. The bioactivity of heparin results from its ability to attract and bind diverse bioavailable molecules, including proangiogenic growth factors (Chiodelli et al., 2015). Thus, the recent works carried out by also our group showed that heparin integrated tissue engineered scaffolds promote angiogenesis (Feng et al., 2017; Kocak et al., 2020, 2022b; Sun et al., 2011; Yar et al., 2016, 2017).

In our recent studies, in situ formed injectable hybrid hydrogels have been developed for bone regeneration and drug delivery. These hydrogels were constituted based on a CS matrix used as a biodegradable and thermo-gelling polymer (at body temperature) which was incorporated with bioactive carbonated HA as inorganic bone matrix and bioactive Hep for proangiogenic purposes (Kocak et al., 2020, 2022b). This present study involves further characterizations of these CS-HA-Hep hydrogels which was formed by a sterile sol–gel method when glycerol has been added to control sol and gel properties, for example, increasing pH level during addition of $NaHCO_3$ by delaying precipitation point for obtaining homogeneous solution, enhancement of physical crosslinking and mechanical strength. The further characterizations in this study involve investigation of in vitro swelling, degradation, and bioactivity capacities of CS-HA-Hep hydrogels. The swelling of hydrogels, which impacts degradation and drug delivery, has been investigated in phosphate-buffered saline (PBS) at 7.4 pH. Biomineralization by deposition of carbonated apatite crystals on hydrogels was investigated by immersion of hydrogels in SBF. Biodegradation through hydrolysis and enzyme activities were investigated by taking a model of biomimetic degradation of chitosan by lysozyme enzyme (Lys.). Hydrogels were tested for degradation by immersion in PBS in the presence and absence of Lys. The complementary chemical and morphological analyses involved pH and weight measurements, and Fourier transform infrared-attenuated total reflectance (FTIR-ATR), scanning electron microscopy (SEM), and energy dispersive spectroscopy (EDS) analyses.

2 | MATERIALS AND METHODS

2.1 | Materials

For synthesis of hydrogels, chitosan (medium Mw: 100–300 kDa, DDA: ≥90%), glycerol (99%), and acetic acid (glacial) were supplied from ACROS Organics™ (Thermo Fisher Scientific) and sodium bicarbonate ($NaHCO_3$) from Fluka® (Sigma Aldrich). Sodium Heparin (from bovine source; injectable grade, 156 IU/mg of activity) was kindly provided as a gift from Extrasul-Ext. An. Veg. Ltda. In all experiments, de-ionized ultrapure (Type-I) water ($D.H_2O$) (Veolia Water Technologies, PURELAB® Chorus, 18.2 MΩ cm) was utilized.

2.2 | Synthesis of injectable hydrogels

CS/HA/Hep hydrogels were synthesized according to the procedure we reported previously (Kocak et al., 2022b). Briefly, CS powder (5%, w/v) was suspended in $D.H_2O$ containing 5% (wt./v) of glycerol. Then, it was dissolved by dropwise addition of 0.5 M of acetic acid. Hydroxyapatite powders synthesized as earlier reported (Kocak, 2021; Kocak et al., 2022a) have been mixed thoroughly into CS solution (HA/CS: 1/10) by stirring for 24 h. The Hep was dissolved in $D.H_2O$ (5 mL) and slowly added to the CS/HA blend. The viscous solution of CS/HA/Hep was then neutralized by addition of 0.48 M of $NaHCO_3$ drop-by-drop in an ice bath. Injectable solutions were obtained and incubated at 37°C for 48 h in glass dishes with lids to obtain stable hydrogels. Hydrogel samples in different compositions, including sole CS (CI), CS + HA (CII), and CS + HA + Hep (SI) (120 μg/mL of Hep in final neutral solution), were synthesized and symbolized as given in parenthesis (CI, CII, and SI). For different analyses, hydrogel specimens were prepared by cutting with cork-borers in different diameters for swelling and degradation (Ø: 5/16 inch) and bioactivity (Ø: 1/4 inch) analyses.

2.3 | Swelling (liquid absorption) tests

The initial weight of each hydrogel specimen (three sample replicates and $n = 3$) was weighted and recorded as W_i (~0.1 g). The samples were then placed in vials containing 3 mL of PBS media and incubated at 37°C. At different time intervals of 30 min, and 1, 2, 4, 6, 15, 24, 48, and 72 h, after removing their surface water, samples were weighed again and recorded as W_s. The percentage of swelling was counted by the given formula (Equation 1) where W_i and W_s represent the initial and swollen weights of hydrogels, respectively.

$$\text{swelling ratio}(\%) = (W_s - W_i)/W_i \times 100. \quad (1)$$

2.4 | In vitro degradation tests

For degradation studies, PBS tablets (Dulbecco A, pH 7.3 ± 0.2 at 25°C) (Thermo Scientific™, Oxoid™) and lysozyme from hen egg white (≤20,000 U/mg, Thermo Fisher Scientific™, MP Medical™) were utilized. Hydrogels (four sample replicates and $n = 3$) were weighed (~0.1 g) and recorded as W_i as initial mass. Samples in two groups were prepared by incubating (at 37°C) in 3 mL of PBS and PBS + lysozyme (5 mg/mL). The sample vials were manually swirled twice a day and the media refreshed every 3 days. At determined time intervals (1, 3, 7, 14, 21, 28, 35, and 42 days), pH of media was measured for each specimen of both groups. Samples were washed with $D.H_2O$ to remove adsorbed ions and incubated at 37°C for 24 h. Then, samples were weighed and recorded as (Wt). The percentage weight loss was calculated by using Equation (2). For degradation time intervals of 14, 28, and 42 days, the freeze-dried samples were analyzed by FTIR-ATR and SEM.

$$\text{weight loss}(\%) = (W_i - W_t)/W_i \times 100. \quad (2)$$

2.5 | Bioactivity studies by SBF

For SBF preparation, the following chemicals were supplied: NaCl, $NaHCO_3$, KCl, $K_2HPO_4.2H_2O$, $MgCl_2.6H_2O$, $CaCl_2$, and Na_2SO_4 from Sigma-Aldrich®, and 1 N HCl and $(CH_2OH)_3CNH_2$ (Tris) from Thermo

Fisher Scientific™ (ACROS Organics™). The SBF solution was prepared at a pH of 7.4 at 36.5°C as reported in the literature (Kokubo & Takadama, 2006). Hydrogel specimens were prepared in triplicates as $n = 3$. The initial weights of samples were measured and recorded as W_i (~0.05 g). Then, the specimens were incubated (at 37°C) in universal test tubes containing 10 mL of SBF media. At determined intervals (7, 14, and 21 days), pH of each specimen media was measured. Hydrogels were washed thrice, and surface water was removed. Then, each sample was weighed and recorded as W_i. Following this, samples were freeze-dried, weighed again, and recorded as W_{fd}. Dry weight ratio in percentage was counted for each sample by using Equation (3). The freeze-dried samples were then further analyzed by SEM, EDS, and FTIR-ATR for each time interval.

$$\text{dry weight ratio}(\%) = W_{fd}/W_i \times 100. \quad (3)$$

2.6 | Statistical analyses

Statistical analyses were carried out by using two-way ANOVA-Tukey multiple comparison tests performed ($p \leq 0.05$ was assessed as statistically significant).

3 | RESULTS AND DISCUSSIONS

3.1 | Swelling tests by weight and Ph analyses

The swelling profile of different hydrogel compositions was investigated by measuring liquid absorption of hydrogels tested with PBS media. The mass change of hydrogels immersed in PBS and the supernatant media pH was measured at determined time slots (0.5, 1, 2, 4, 6, 15, 24, 48, and 72 h). The plots of swelling percentages and pH alteration in immersion media are given in Figure 1. The highest amount of swelling occurred in the first 30 min. Then, liquid absorption was slowly increased and reached to an equilibrium within 6 h (Figure 1a). CS hydrogel (CI) showed a higher portion of swelling over the test time, and the maximum swelling was measured as 68% (wt) at 6 h ime period. CS-HA-Hep samples (SI) indicated the least liquid absorption of 55% at this point. After 15 h, hydrogels showed a slight tendency of de-swelling up to 72 h. The pH values rose gradually by 15 h as parallel to swelling, whereas a decrease at pH values observed at the rest of the experiment which was the sharpest in the CI sample (Figure 1b). The pH patterns for CII and SI sample media were almost the same. The maximum pH value was at around 7.70.

The swelling ratio of hydrogels in comparison to the most reported hydrogel formulations was not very high (Coutinho et al., 2010; Jin et al., 2007, 2009; Shahzad et al., 2015). In one study, CS-based hydrogels integrated with HA neutralized with sodium bicarbonate forming hydrogel upon crosslinking at 37°C showed around 30% of swelling in PBS which reaches to 40% in 3 days (Ressler et al., 2018). The higher initial PBS absorption ratio of hydrogels in the present study could be related to the hierarchial morphology comprising macro- and micro- porosity. The presence of micropores might increase the permeability. Overall moderate swelling of hydrogels might result from a strengthened structure of hydrogels by glycerol additive leading pH adjustment to an upper level providing to acquire homogeneous solutions that have also led to further chain entanglement and increase in mechanical strength (Kocak et al., 2022b).

An injectable hydrogel system does not require post-loading of drugs into hydrogels, as these can be added into liquid hydrogel forms directly and bound within the hydrogel networks upon in situ fast gelation. Therefore, a high ratio of swelling for drug loading efficiency is not a prerequisite in these systems.

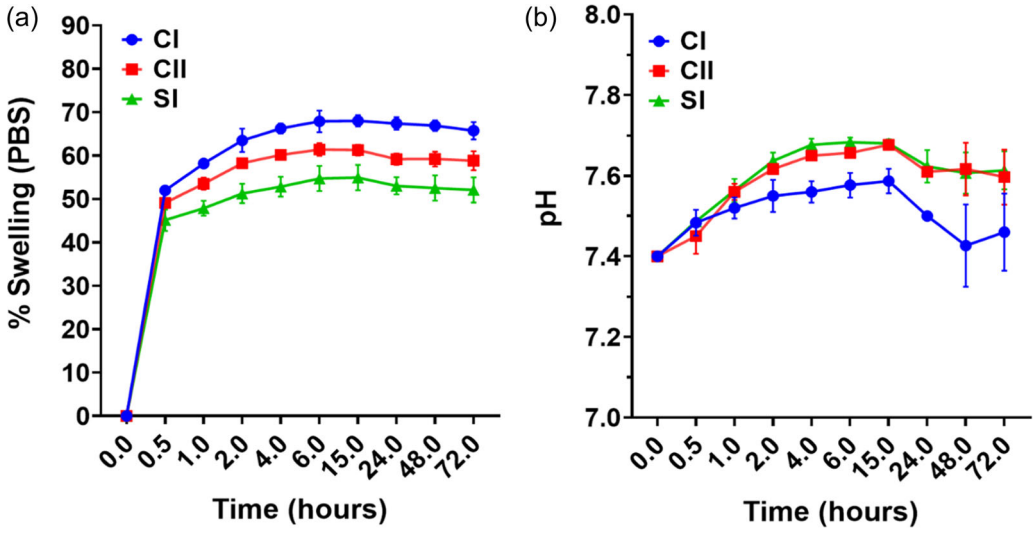

FIGURE 1 The swelling analyses of hydrogels (CI, CII, and SI) at different time intervals: 30 min, and 1, 2, 4, 6, 15, 24, 48, and 72 h: (a) swelling percentage of hydrogels and (b) pH of phosphate-buffered saline (PBS) media that hydrogels were incubated.

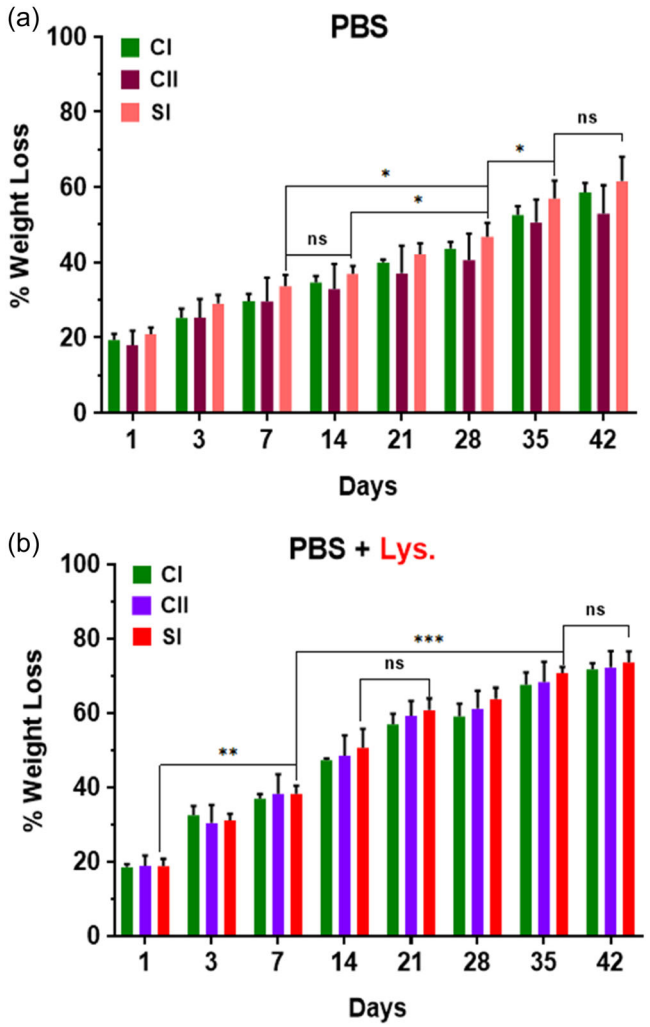

FIGURE 2 The in vitro degradation weight analyses with standard error bars plotted as percentage weight loss in hydrogels (CI, CII, and SI) versus time (up to 42 days) measured for samples incubated in (a) PBS and (b) PBS + Lysozyme (5 mg/mL) solution.

3.2 | In vitro degradation tests

For in vitro degradation tests, hydrogels were incubated in PBS and Lys. (5 mg/mL) + PBS over the 6 weeks. At certain time intervals of tests, weight and pH measurements, and morphological and chemical analyses were carried out.

3.2.1 | Weight and pH analyses at in vitro degradation tests

The weight loss of hydrogels was measured and plotted as a percentage versus time intervals of the test (1, 3, 7, 14, 21, 28, 35, and 42 days) given in Figure 2. In the first 24 hours, approximately 20% of weight loss occurred in all hydrogels for both groups. This high amount of weight decreases after 24 h is presumed to be caused by water loss due to progression of gelation by heating at 37°C for drying. After 2 weeks, in PBS and PBS+Lys. media specimens, around 40% and 50% of weight loss occurred, respectively, which was attributed to polymer dissolution rather than degradation. In the rest of tests, hydrogels have started degradation in a gradual manner reaching 70% of their initial weights after 6 weeks (Figure 2b). The sample group incubated in PBS indicated degradation in a lower speed, which was approximately 35% of weight loss in 14 days, and degradation progressed and amounted to 60%(wt) at the end of tests (Figure 2a). The difference of degradation profile in two different media has not exhibited statistical significance (p: 0.0959), but the degradation rate between the time slots was found to be significant ($p < 0.0001$).

The pH alteration in supernatant media of hydrogels exposing to degradation in PBS and PBS+Lys. has comparatively given in Figure 3. The addition of Lys. in PBS solution has led to a decrease of the initial pH from 7.4 to 7.0–7.1. The pH values of both media groups showed a soar up to 3 days which could be due to liquid absorption. From Day 3 to Day 7, the mean pH values indicated a decrease reaching around 7.3 and 6.9 for PBS and PBS+Lys. media, respectively. A gradual decrease of pH was maintained in the PBS group by 21 days followed by small rises and reductions. However, the sharper changes at pH occurred in PBS+Lys. media, which could be due to interactions of Lys. with CS leading to the more effective breakdown of CS into smaller chains. During the experiments, pH range seems to be mostly in a neutral range which is compatible with physiological pH conditions (Chenite et al., 2000).

3.2.2 | FT-IR analyses at in vitro degradation tests

The chemical structural changes of degrading hydrogels incubated in PBS and PBS+Lys. were analyzed by Fourier Transform Infrared-Attenuated Total Reflectance (FTIR-ATR) Spectroscopy. The analyses were performed for untreated samples (Day 0), and samples exposed to incubation in two different media for 14, 28, and 42 days. The results are given in Figure 4. Over the degradation period, marked reductions occurred in the peak intensities within the region belonging to O–H and N–H groups (3200–3500 cm^{-1}), and the peak intensities were decreased between 2800 and 3000 cm^{-1}, which were contributed to C–H stretching bonds (Shahzad et al., 2015). The decrease at C–O cyclic stretching frequencies (at 1078 cm^{-1}) (Rokhade et al., 2007) was more obvious for Day 28 and Day 42 samples. In addition, the peak intensities at 1416 and 1383 cm^{-1} assigned to CH_2 bending vibrations have explicitly declined with degradation (Shahzad et al., 2015). The peaks located at 1579 cm^{-1} corresponded to amide II or N–H bending deformation, and 1641 cm^{-1} attributed to amide I or C=O linkages (Shahzad et al., 2015; Yar et al., 2017). An increase in the peak intensities at 1649 cm^{-1}

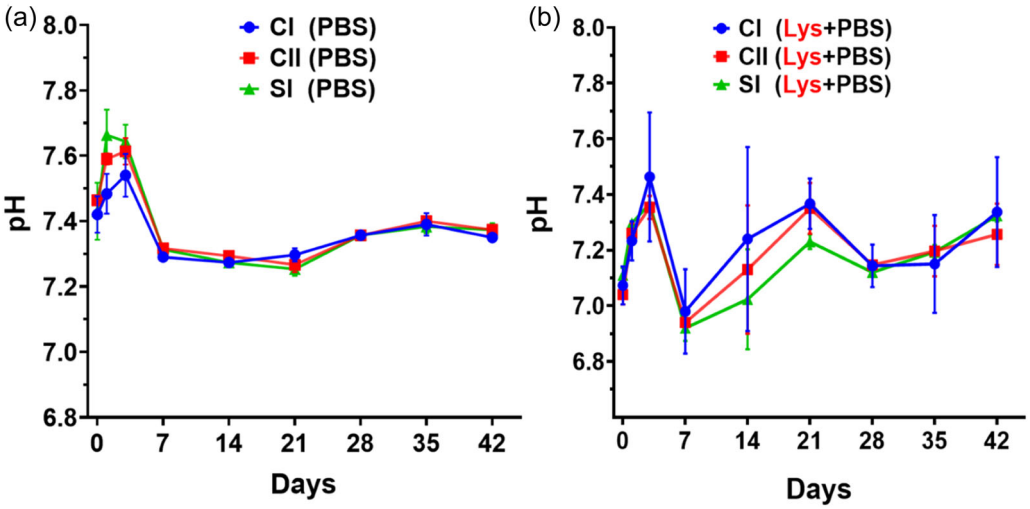

FIGURE 3 The pH alteration at the incubation media of hydrogels (CI, CII, and SI): (a) phosphate-buffered saline (PBS) and (b) lysozyme added PBS (5 mg/mL) (Lys+PBS), plotted versus time up to 42 days of degradation test.

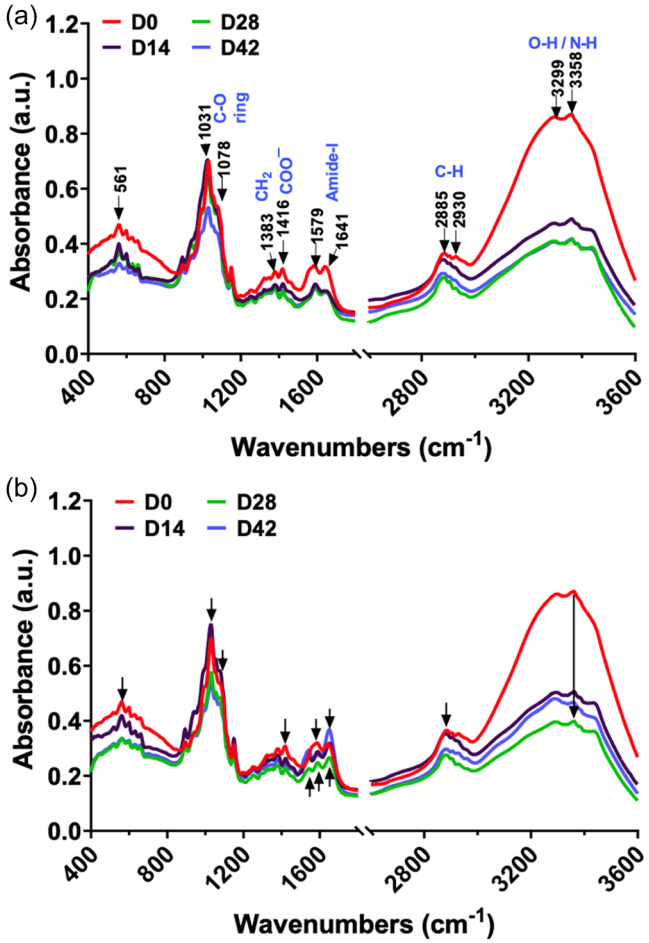

FIGURE 4 The FTIR-ATR analyses of SI hydrogel composition incubated in (a) phosphate-buffered saline (PBS) media and (b) lysozyme added PBS (5 mg/mL): symbolized as (PBS) and (Lys), respectively, in legends on the plots. In legends: Day 0 represents nontreated hydrogels as Day 14, 28, and 42 represent degradation time of samples in a media.

attributed to amide-I linkages has indicated the chemical interactions of lysozyme with CS (Mizuguchi et al., 1997).

3.2.3 | SEM analyses at in vitro degradation tests

SEM morphological analyses of hydrogels were performed at certain degradation periods (14, 28, and 42 days). The degradation samples were tested after the freeze-drying process. Hydrogel specimens have indicated some cracks at Day 14. There were signs of bulk degradation in Day 28 samples for both groups, and this was more obvious in cross-sectional images (Figure 5). In addition, flat top and bottom surfaces were exposed to erosion and the inner layers of CS with micropores were uncovered (Figure 5f,i). Further progress of bulk degradation was seen at Day 42 samples, with large cracks and breaking down of most of the polymeric structure.

It has been reported in literature that degradation speed depends on multi-parameters, including inherent properties of polymers, for example, Mw and DDA of CS, and topological properties, such as porosity, structure of pores, hydrophilic or hydrophobic nature (Jennings, 2017; Qasim et al., 2017). The gradual degradation rate in all hydrogel compositions with no significant difference occurred reaching to around 60% and 70% (wt%) in PBS and PBS+Lys, media, respectively. Our results are comparable with the in vitro degradation test results reported for 4 weeks (around 45%) for HA integrated CS-based hydrogels neutralized with β-glycerophosphate (Liu et al., 2014). In addition, CS-based hydrogels neutralized with $NaHCO_3$ and incorporated with HA by the in situ precipitation technique have been reported. The in vitro degradation results of these hydrogels were parallel with our study showing around 30% of weight loss in 3 days. Faster degradation of our hydrogels with approximately 10% higher weight loss was observed at Day 14 and Day 28 studies. This could be related to a higher concentration of lysozyme used in our study

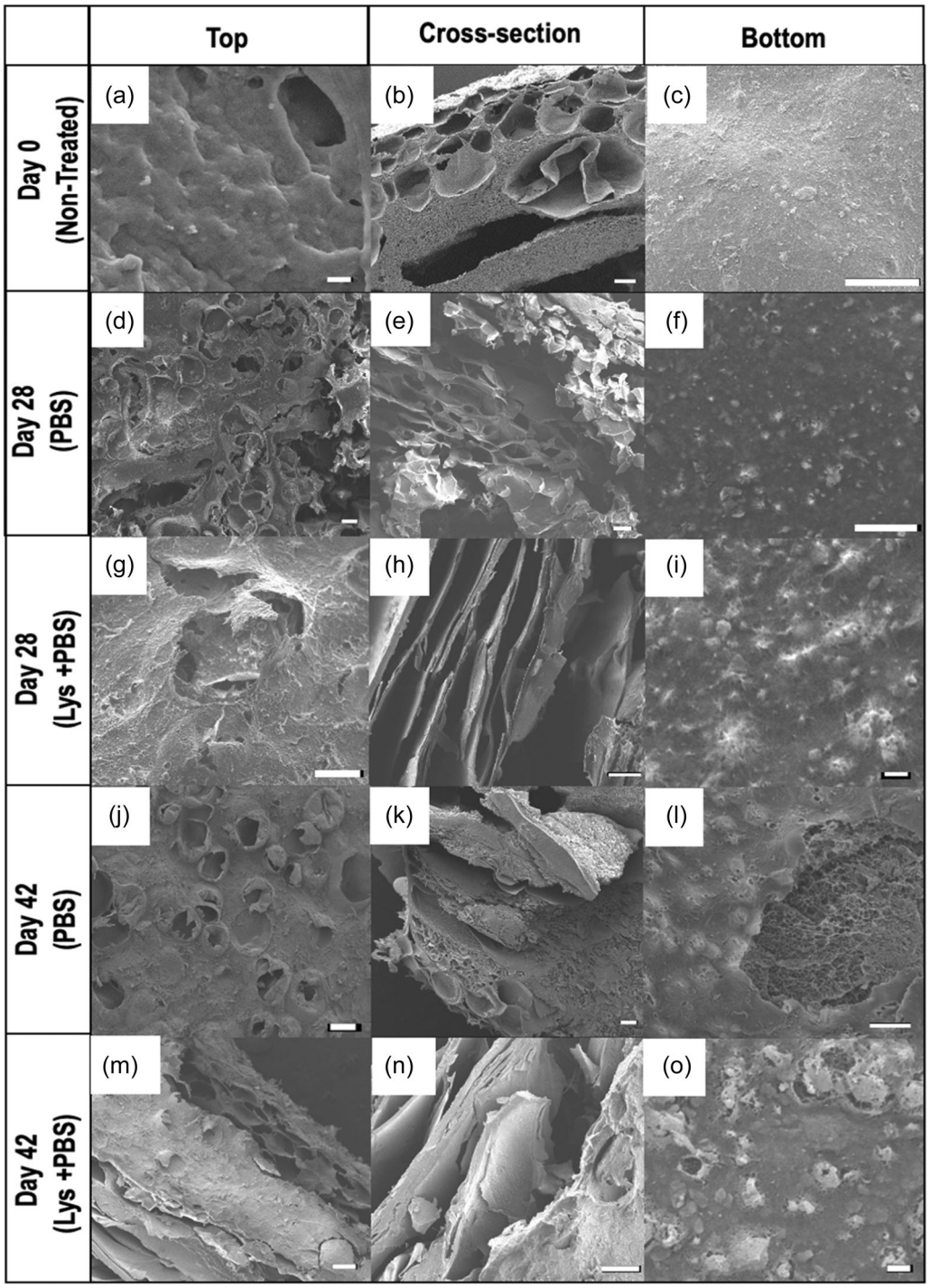

FIGURE 5 Comparative SEM images of composite hydrogels (SI) during degradation in phosphate-buffered saline (PBS) and lysozyme added PBS (5 mg/mL) media. The micrographs from left to right in three columns show top, cross-section, and bottom sites. The vertical labels indicate the day of degradation test and the used media. Day 0 labeled images (a–c) represent hydrogels before media treatment. Scale bars at the following images represent: (b–e; g, h; j, k; m, n): 100 µm, (f, l): 10 µm and (a, I, o): 1 µm.

(Ressler et al., 2018), as it has been reported that in vitro and in vivo degradation rates may differ. In addition, following an implant placement, time required for formation of new bones has been reported to start within 1–2 months (Danilchenko et al., 2011; Qasim et al., 2017).

3.3 | Bioactivity tests in SBF

After sequent time intervals, the chemical and morphological analyses of SBF-treated hydrogels were conducted by pH and weight measurements, and ATR, SEM, and EDS analyses.

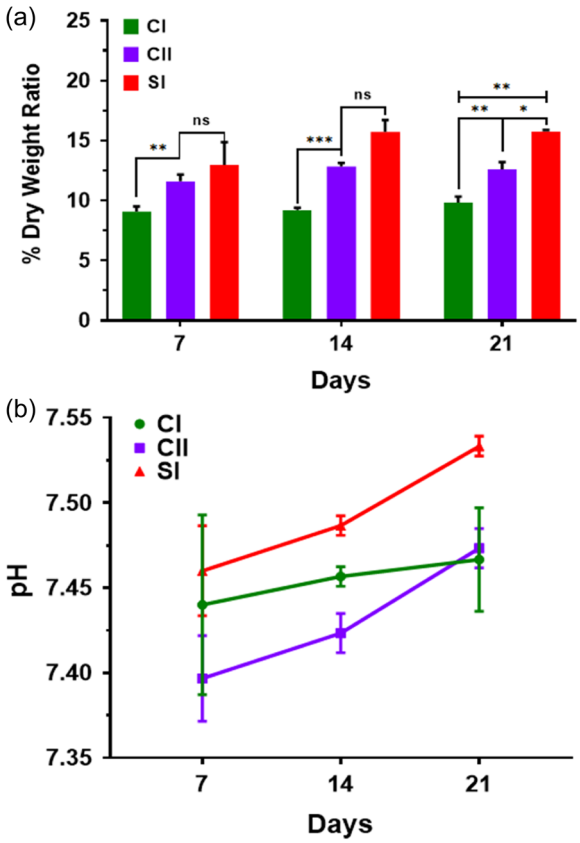

FIGURE 6 The bioactivity analyses of hydrogels (CI, CII, and SI) with standard errors plotted versus time up to 21 days (7, 14, and 21 days): (a) dry weight ratio of hydrogels in as percentage and (b) pH changes in the SBF media at test times.

3.3.1 | Weight and pH analyses at bioactivity tests

Mineralization capacity by weight was measured and plotted as dry mass percentage of hydrogels versus time of incubation in SBF (for 7, 14, and 21 days). The pH values of supernatant SBF media were measured and compared for sample compositions and time intervals. The results are given comparatively in Figure 6. In pH analyses, a rise tendency of pH in media of specimens was measured in all samples from Day 7 to Day 21 (Figure 6b). The highest values of the mean media pH possessed by the SI sample were between 7.46 and 7.53.

Upon 7 days of treatment with SBF, the composite hydrogels, CII, and SI indicated formation of white hardened mineral layer on top surfaces visibly. However, the basic CS hydrogels (CI) without HA and Hep had almost no visible or weight-based mineralization. The total dry weight ratio change in the CI sample was only 0.7% from Day 7 to Day 21. At Day 7, the CII sample showed significantly higher mineralization than the CI. The highest mineralization by weight belongs to the SI sample at all time intervals while no statistical difference was observed between CII and SI at Days 7 and 14 (Figure 6a).

An increment in the dry mass percentage of CII and SI samples was 1.4% and 2.5% (wt%), respectively, from Day 7 to Day 14, whereas almost no change occurred between 14 and 21 days. At Day 21, the composite SI sample showed the highest degree of mineralization, which was statistically higher than CII ($p = 0.0183$). These results revealed the contribution of Hep to bioactivity of hydrogels as well as HA in a longer term. Hence, it could be stated that heparin had an impact on bioactivity not only by binding proangiogenic molecules biologically but also ions in SBF inducing apatite forming capacity required for bone regeneration. It was reported that integration of Hep into fibrinogen-based injectable gels promoted alkaline phosphatase activity leading to mineralization (Yang et al., 2010). Moreover, poly-caprolactone (PCL) membranes functionalized with Hep was reported to improve alkaline phosphatase activity for osteogenic differentiation (Gümüşderelioğlu et al., 2011). There are not many studies discussing the effect of Hep on in vitro mineralization in SBF. However, it is reported that Hep has been used to adjust crystalline properties of calcium phosphates (Park et al., 2018). Furthermore, attraction of Ca^{2+} ions by anionic groups in Hep (COO^- and SO_3^-) has led to a high Ca/P ratio leading to apatite deposition in alkaline conditions in carbonated apatite regulated by heparin (Deng et al., 2013).

3.3.2 | SEM AND EDS analyses at bioactivity tests

The morphological analyses of SBF-treated hydrogels were performed on lyophilized samples by SEM. To determine elemental composition, mineralized top surface of hydrogels was analyzed by area mapping in EDS. The SEM and EDS results of samples are demonstrated comparatively in Figure 7.

EDS, compositional analyses of CI belonging to CS hydrogel matrix included the elements of C, O and N, and Na (from a neutralizing agent) (Figure 7a). After 7 days of SBF treatment, EDS data of CS were similar and no-detection of Ca and P elements was observed (Figure 7d). Before SBF treatment, composite CII and SI samples possessed additional Ca and P elements due to the presence of HA (Figure 7b,c). Upon SBF treatment (7 days), much higher intensities of Ca and P peaks were detected showing apatite mineralization (Figure 7e,f). The ratio of Ca/P showed variability between samples and incubation days. The detected trace elements, such as Cl and Mg could be the attached ions due to SBF treatments, and the presence of Au was due to conductive coating before SEM imaging.

The SEM image of CI sample after 14 days of SBF treatment had a soft, flat non-mineralized surface (Figure 7g). However, the CII sample (CS + HA) possessed a quite rough surface with a deposition of flower-like, needle-shaped crystals of carbonated apatite on the surface and within the porous structure of hydrogels observed at cross-sectional areas (Figure 7h). A distinct morphological structure was also observed with SI sample (CS + HA + Hep) that possesses a soft coating layer of Hep in which the crystalline apatite layer has embedded below (Figure 7i).

The physical indication of mineralization was also shown in the photographs in Figure 8 demonstrating hydrogel specimens before SBF treatment and after 14 days of SBF treatment (upon freeze-drying). As

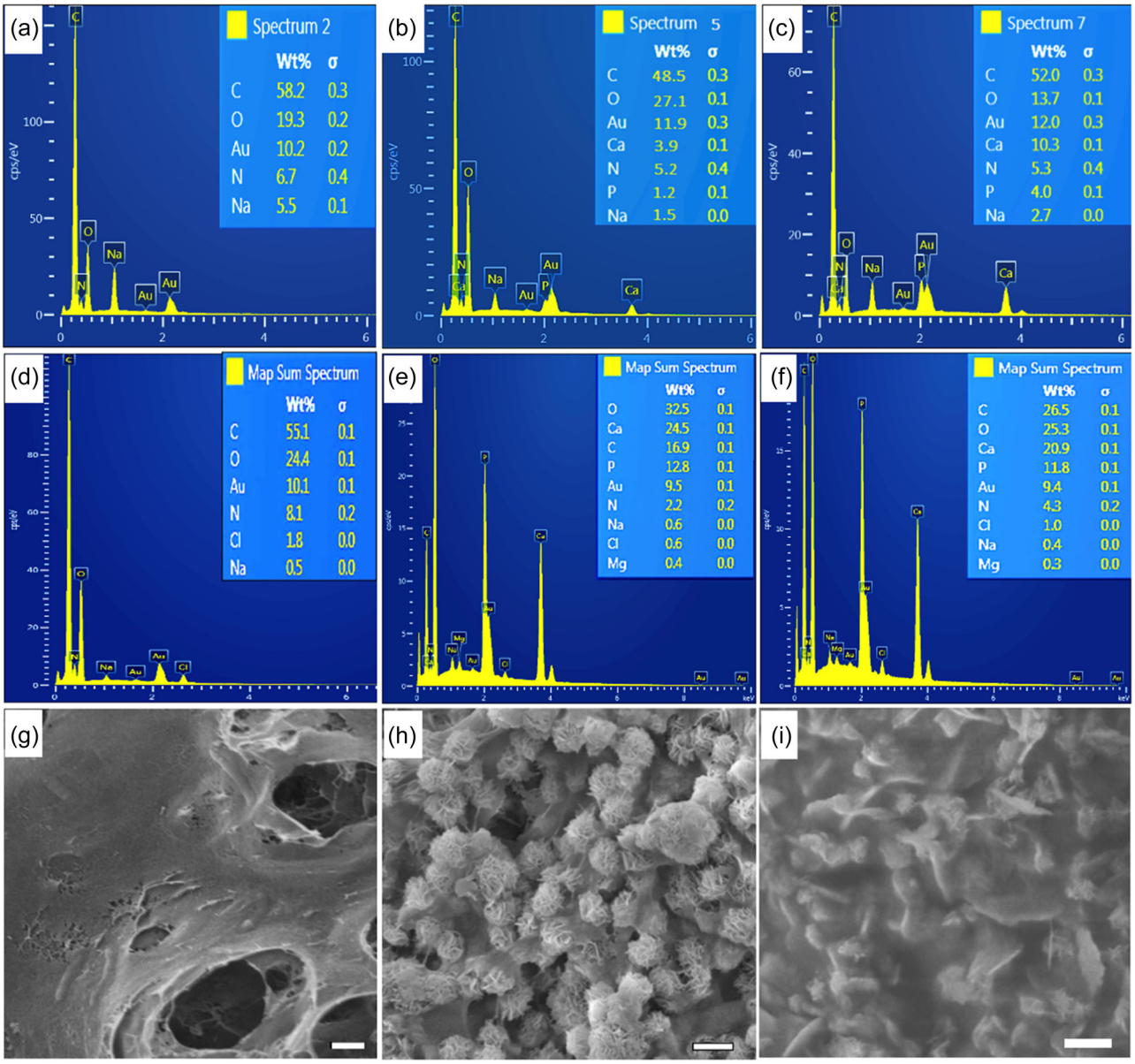

FIGURE 7 Energy dispersive spectroscopy (EDS) analyses of (a–c) hydrogels: CI, CII, and SI, respectively (scale bars are 1 μm) before simulated body fluid (SBF) treatment and (d–f) after 7 days of SBF treatment and (g–i) SEM images of those hydrogels treated in SBF for 14 days at their freeze-dried forms.

can be seen in Figure 8, after 14 days of SBF treatment, top surfaces of composite hydrogels had white mineral layer deposition, whereas sole CS sample and the bottom surfaces of all samples lacked mineralized layer. The mineral surface of the SI sample (CS + HA + Hep) was softer than that of CII (CS + HA) which is considered due to the coating effect of Hep positioning itself at top. The results were also confirmed by SEM and EDS analyses in Figure 7.

3.3.3 | FT-IR analyses at bioactivity tests

The FTIR-ATR analyses were performed on freeze-dried hydrogels after treating with SBF for 7 days and nontreated (Day 0) samples as control, and spectral results were comparatively presented in Figure 9. In SBF-treated composite samples, rise of an intense peak locating at 1018 cm^{-1} was attributed to v_3 bond of PO_4^{-3} linkages due to asymmetric stretching frequencies. This peak dominated other peaks present in the basic CS sample (CI), locating at the region between 800 and 1200 cm^{-1}. Another PO_4^{-3} bond in v_1-symmetric stretching mode appeared at 963 cm^{-1} at the spectral data of composite hydrogels (CII and SI). In addition, a relatively small peak observed at 878 cm^{-1} is due to B-type carbonate substitution in apatite structures. Furthermore, v_4-type crystalline PO_4^{-3} linkages in the spectra were observed at 558 and 600 cm^{-1} (Antonakos et al., 2007; Gibson & Bonfield, 2002).

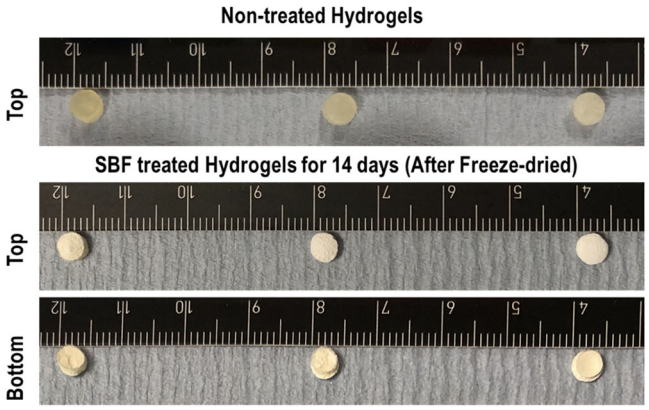

FIGURE 8 The photographs of hydrogels before simulated body fluid (SBF) treatment: CI, CII, and SI from left to right are given at top. The photographs of hydrogels after treated in SBF for 14 days followed by freeze drying are given below (mineralized top and non-mineralized bottom surfaces are seen in composite samples, while the sole CS sample showed almost no mineralization in both sides).

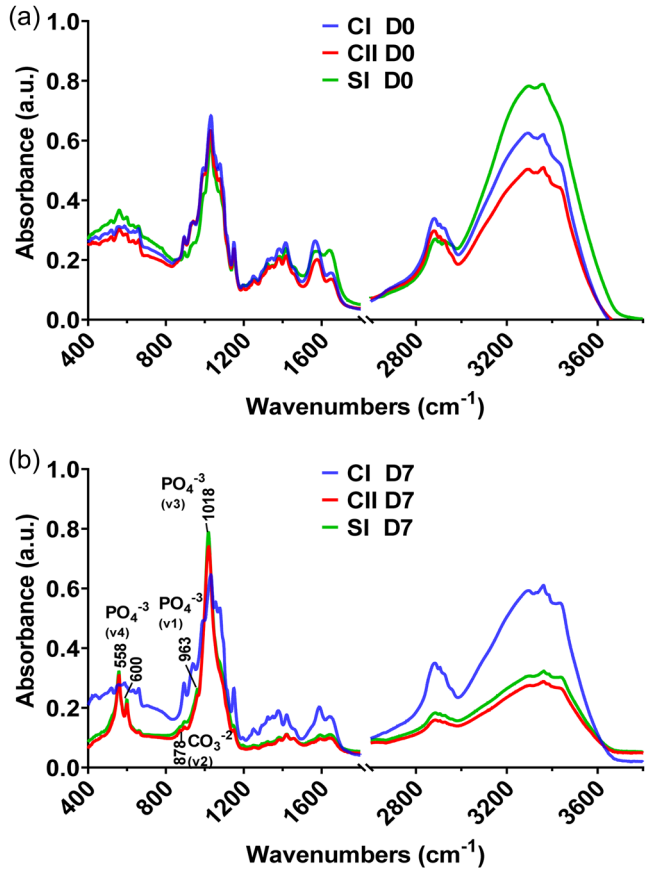

FIGURE 9 The Fourier transform infrared-attenuated total reflectance analyses of different hydrogel compositions (CI, CII, and SI) which were analyzed after freeze-drying for (a) hydrogels which were not treated with SBF (b) hydrogels were incubated in SBF at 37°C for 7 days.

4 | CONCLUSIONS

This study has investigated in vitro swelling, degradation, and bioactivity properties of in situ forming injectable natural CS matrixed hydrogels integrated with bioactive HA and proangiogenic Hep (CS-HA-Hep) produced with glycerol addition. Hydrogels having a hierarchical morphology showed respectively low ratio of swelling which can be suitable for controlled drug release applications. Hydrogels exposed to gradual degradation in PBS with the presence and absence of lysozyme over 6 weeks. The bioactivity results with SBF showed that injectable hydrogels showed unique bioactive features not only provided by HA but also significantly enhanced by the presence of Hep in composite hydrogels at longer duration (e.g., 21 days). Together with previously investigated injectability (allowing proper injection by 21-gauge and wider needles), in situ quick gelation (2–3 min), biocompatibility, and stimulation of angiogenesis in chick embryos, these functionalized bioactive and biodegradable hybrid hydrogels seem potential candidates for further clinical studies on minimally invasive bone regeneration and therapeutic delivery applications.

AUTHOR CONTRIBUTIONS

Fatma Zehra Kocak: Conceptualization; methodology; investigation; writing—original draft. **Muhammad Yar**: Conceptualization; methodology; reviewing and editing; supervision. **Ihtesham Ur Rehman**: Conceptualization; methodology; reviewing and editing; supervision; project administration.

ACKNOWLEDGMENTS

The authors thank to Extrasul Ext. An. Veg. Ltda (Sao Paulo, Brazil) for kind gift of sodium bovine heparin. This research was supported by the "Turkish Ministry of National Education".

DATA AVAILABILITY STATEMENT

The data that support the findings of this study are available from the corresponding author upon reasonable request.

ORCID

Fatma Zehra Kocak http://orcid.org/0000-0001-6397-322X

REFERENCES

Aleem, A. R., Shahzadi, L., Alvi, F., Khan, A. F., Chaudhry, A. A., ur Rehman, I., & Yar, M. (2017). Thyroxin releasing chitosan/collagen based smart hydrogels to stimulate neovascularization. *Materials & Design*, *133*, 416–425. https://doi.org/10.1016/j.matdes.2017.07.053

AL-Hamoudi, F., Rehman, H. U., Almoshawah, Y. A., Talari, A. C. S., Chaudhry, A. A., Reilly, G. C., & Rehman, I. U. (2022). Bioactive composite for orbital floor repair and regeneration. *International Journal of Molecular Sciences*, *23*(18), 10333. https://doi.org/10.3390/ijms231810333

Amini, A. R., Laurencin, C. T., & Nukavarapu, S. P. (2012). Bone tissue engineering: Recent advances and challenges. *Critical Reviews in Biomedical Engineering*, *40*(5), 363–408. https://doi.org/10.1111/j.1743-6109.2008.01122.x.Endothelial

Antonakos, A., Liarokapis, E., & Leventouri, T. (2007). Micro-Raman and FTIR studies of synthetic and natural apatites. *Biomaterials*, *28*(19), 3043–3054. https://doi.org/10.1016/j.biomaterials.2007.02.028

Arun Kumar, R., Sivashanmugam, A., Deepthi, S., Iseki, S., Chennazhi, K. P., Nair, S. V., & Jayakumar, R. (2015). Injectable chitin-poly(ε-caprolactone)/nanohydroxyapatite composite microgels prepared by simple regeneration technique for bone tissue engineering. *ACS Applied Materials & Interfaces*, *7*(18), 9399–9409. https://doi.org/10.1021/acsami.5b02685

Bedi, R. S., Chow, G., Wang, J., Zanello, L., & Yan, Y. S. (2012). Bioactive materials for regenerative medicine: Zeolite-hydroxyapatite bone mimetic coatings. *Advanced Engineering Materials*, *14*(3), 200–206. https://doi.org/10.1002/adem.201100170

Chaudhry, A. A., Knowles, J. C., Rehman, I., & Darr, J. A. (2013). Rapid hydrothermal flow synthesis and characterisation of carbonate- and silicate-substituted calcium phosphates. *Journal of Biomaterials Applications*, *28*(3), 448–461. https://doi.org/10.1177/0885328212460289

Chenite, A., Chaput, C., Wang, D., Combes, C., Buschmann, M. D., Hoemann, C. D., Leroux, J. C., Atkinson, B. L., Binette, F., & Selmani, A. (2000). Novel injectable neutral solutions of chitosan form biodegradable gels in situ. *Biomaterials*, *21*(21), 2155–2161. https://doi.org/10.1016/S0142-9612(00)00116-2

Chiodelli, P., Bugatti, A., Urbinati, C., & Rusnati, M. (2015). Heparin/heparan sulfate proteoglycans glycomic interactome in angiogenesis: Biological implications and therapeutical use. *Molecules*, *20*(4), 6342–6388. https://doi.org/10.3390/molecules20046342

Chuysinuan, P., Nooeaid, P., Thanyacharoen, T., Techasakul, S., Pavasant, P., & Kanjanamekanant, K. (2021). Injectable eggshell-derived hydroxyapatite-incorporated fibroin-alginate composite hydrogel for bone tissue engineering. *International Journal of Biological Macromolecules*, *193*(PA), 799–808. https://doi.org/10.1016/j.ijbiomac.2021.10.132

Coutinho, D. F., Sant, S. V., Shin, H., Oliveira, J. T., Gomes, M. E., Neves, N. M., Khademhosseini, A., & Reis, R. L. (2010). Modified Gellan Gum hydrogels with tunable physical and mechanical properties. *Biomaterials*, *31*(29), 7494–7502. https://doi.org/10.1016/j.biomaterials.2010.06.035

Danilchenko, S. N., Kalinkevich, O. V., Pogorelov, M. V., Kalinkevich, A. N., Sklyar, A. M., Kalinichenko, T. G., Ilyashenko, V. Y., Starikov, V. V., Bumeyster, V. I., Sikora, V. Z., & Sukhodub, L. F. (2011). Characterization and in vivo evaluation of chitosan-hydroxyapatite bone scaffolds made by one step coprecipitation method. *Journal of biomedical materials research. Part A*, *96 A*(4), 639–647. https://doi.org/10.1002/jbm.a.33017

Darr, J. a, Guo, Z. X., Raman, V., Bououdina, M., & Rehman, I. U. (2004). Metal organic chemical vapour deposition (MOCVD) of bone mineral like carbonated hydroxyapatite coatings. *Chemical Communications*, *6*, 696–697. https://doi.org/10.1039/b312855p

Deng, A., Kang, X., Zhang, J., Yang, Y., & Yang, S. (2017). Enhanced gelation of chitosan/β-sodium glycerophosphate thermosensitive hydrogel with sodium bicarbonate and biocompatibility evaluated. *Materials Science and Engineering: C*, *78*, 1147–1154. https://doi.org/10.1016/j.msec.2017.04.109

Deng, Y., Sun, Y., Chen, X., Zhu, P., & Wei, S. (2013). Biomimetic synthesis and biocompatibility evaluation of carbonated apatites template-mediated by heparin. *Materials Science and Engineering: C*, *33*(5), 2905–2913. https://doi.org/10.1016/j.msec.2013.03.016

Dessì, M., Borzacchiello, A., Mohamed, T. H. A., Abdel-Fattah, W. I., & Ambrosio, L. (2013). Novel biomimetic thermosensitive β-tricalcium phosphate/chitosan-based hydrogels for bone tissue engineering. *Journal of Biomedical materials research. Part A*, *101*(10), 2984–2993. https://doi.org/10.1002/jbm.a.34592

Do, N. H. N., Truong, Q. T., Le, P. K., & Ha, A. C. (2022). Recent developments in chitosan hydrogels carrying natural bioactive compounds. *Carbohydrate Polymers*, *294*(June), 119726. https://doi.org/10.1016/j.carbpol.2022.119726

Dubnika, A., & Zalite, V. (2014). Preparation and characterization of porous Ag doped hydroxyapatite bioceramic scaffolds. *Ceramics International*, *40*(7 PART A), 9923–9930. https://doi.org/10.1016/j.ceramint.2014.02.088

Feng, Y., Li, Q., Wu, D., Niu, Y., Yang, C., Dong, L., & Wang, C. (2017). A macrophage-activating, injectable hydrogel to sequester endogenous growth factors for in situ angiogenesis. *Biomaterials*, *134*, 128–142. https://doi.org/10.1016/j.biomaterials.2017.04.042

Gibson, I. R., & Bonfield, W. (2002). Novel synthesis and characterization of an AB-type carbonate-substituted hydroxyapatite. *Journal of Biomedical Materials Research*, *59*(4), 697–708. https://doi.org/10.1002/jbm.10044

Gümüşderelioğlu, M., Karakeçili, A., & Demirtaş, T. T. (2011). Osteogenic activities of MC3T3-E1 cells on heparin-immobilized poly(caprolactone) membranes. *Journal of Bioactive and Compatible Polymers*, *26*(3), 257–269. https://doi.org/10.1177/0883911511406329

Hoemann, C. D., Sun, J., Légaré, A., McKee, M. D., & Buschmann, M. D. (2005). Tissue engineering of cartilage using an injectable and adhesive chitosan-based cell-delivery vehicle. *Osteoarthritis and Cartilage*, *13*(4), 318–329. https://doi.org/10.1016/j.joca.2004.12.001

Iqbal, H., Ali, M., Zeeshan, R., Mutahir, Z., Iqbal, F., Nawaz, M. A. H., Shahzadi, L., Chaudhry, A. A., Yar, M., Luan, S., Khan, A. F., & Rehman, I. (2017). Chitosan/hydroxyapatite (HA)/hydroxypropylmethyl cellulose (HPMC) spongy scaffolds-synthesis and evaluation as potential alveolar bone substitutes. *Colloids and Surfaces B: Biointerfaces*, *160*, 553–563. https://doi.org/10.1016/j.colsurfb.2017.09.059

Jennings, J. A. (2017). Controlling chitosan degradation properties in vitro and in vivo. *In Chitosan Based Biomaterials*, *1*, 159–182. https://doi.org/10.1016/B978-0-08-100230-8.00007-8

Jin, R., Hiemstra, C., Zhong, Z., & Feijen, J. (2007). Enzyme-mediated fast in situ formation of hydrogels from dextran-tyramine conjugates. *Biomaterials*, *28*(18), 2791–2800. https://doi.org/10.1016/j.biomaterials.2007.02.032

Jin, R., Moreira Teixeira, L. S., Dijkstra, P. J., Karperien, M., van Blitterswijk, C. A., Zhong, Z. Y., & Feijen, J. (2009). Injectable chitosan-based hydrogels for cartilage tissue engineering. *Biomaterials*, *30*(13), 2544–2551. https://doi.org/10.1016/j.biomaterials.2009.01.020

Juhasz, J. A., & Best, S. M. (2012). Bioactive ceramics: Processing, structures and properties. *Journal of Materials Science*, *47*(2), 610–624. https://doi.org/10.1007/s10853-011-6063-x

Kocak, F. Z. (2021). *Smart pH and thermosensitive injectable hydrogels: Functionalised biomaterials for bone regeneration*. Lancaster University. https://doi.org/10.17635/lancaster/thesis/1274

Kocak, F. Z., Talari, A. C. S., Yar, M., & Rehman, I. U. (2020). In-situ forming pH and thermosensitive injectable hydrogels to stimulate angiogenesis: Potential candidates for fast bone regeneration applications. *International Journal of Molecular Sciences*, *21*(5), 1633. https://doi.org/10.3390/ijms21051633

Kocak, F. Z., Yar, M., & Rehman, I. U. (2022a). *Investigation of different synthesis parameters of hydroxyapatite for tissue engineering applications*. The sixth international symposium on pharmaceutical and biomedical sciences (ISPBS-6) (pp. 121–126).

Kocak, F. Z., Yar, M., & Rehman, I. U. (2022b). Hydroxyapatite-Integrated, heparin- and glycerol-functionalized chitosan-based injectable hydrogels with improved mechanical and proangiogenic performance. *International Journal of Molecular Sciences*, *23*(10), 53–70. https://doi.org/10.3390/ijms23105370

Kokubo, T., & Takadama, H. (2006). How useful is SBF in predicting in vivo bone bioactivity. *Biomaterials*, *27*(15), 2907–2915. https://doi.org/10.1016/j.biomaterials.2006.01.017

Kong, L., Gao, Y., Lu, G., Gong, Y., Zhao, N., & Zhang, X. (2006). A study on the bioactivity of chitosan/nano-hydroxyapatite composite scaffolds for bone tissue engineering. *European Polymer Journal*, *42*(12), 3171–3179. https://doi.org/10.1016/j.eurpolymj.2006.08.009

Li, F., Liu, Y., Ding, Y., & Xie, Q. (2014). A new injectable in situ forming hydroxyapatite and thermosensitive chitosan gel promoted by Na_2CO_3. *Soft Matter*, *10*(13), 2292–2303. https://doi.org/10.1039/C3SM52508B

Lih, E., Lee, J. S., Park, K. M., & Park, K. D. (2012). Rapidly curable chitosan–PEG hydrogels as tissue adhesives for hemostasis and wound healing. *Acta Biomaterialia*, *8*(9), 3261–3269. https://doi.org/10.1016/j.actbio.2012.05.001

Liu, L., Tang, X., Wang, Y., & Guo, S. (2011). Smart gelation of chitosan solution in the presence of $NaHCO_3$ for injectable drug delivery system. *International Journal of Pharmaceutics*, *414*(1–2), 6–15. https://doi.org/10.1016/j.ijpharm.2011.04.052

Liu, X., Chen, Y., Huang, Q., He, W., Feng, Q., & Yu, B. (2014). A novel thermo-sensitive hydrogel based on thiolated chitosan/hydroxyapatite/beta-glycerophosphate. *Carbohydrate Polymers*, *110*, 62–69. https://doi.org/10.1016/j.carbpol.2014.03.065

Méthot, S., Changoor, A., Tran-Khanh, N., Hoemann, C. D., Stanish, W. D., Restrepo, A., Shive, M. S., & Buschmann, M. D. (2016). Osteochondral biopsy analysis demonstrates that BST-CarGel treatment improves structural and cellular characteristics of cartilage repair tissue compared with microfracture. *Cartilage*, *7*(1), 16–28. https://doi.org/10.1177/1947603515595837

Mizuguchi, M., Nara, M., Ke, Y., Kawano, K., Hiraoki, T., & Nitta, K. (1997). Fourier-transform infrared spectroscopic studies on the coordination of the side-chain COO- groups to Ca2+ in equine lysozyme. *European Journal of Biochemistry*, *250*(1), 72–76. https://doi.org/10.1111/j.1432-1033.1997.00072.x

Najeeb, S., Khurshid, Z., Zafar, M., Khan, A., Zohaib, S., Martí, J., Sauro, S., Matinlinna, J., & Rehman, I. (2016). Modifications in glass ionomer cements: Nano-sized fillers and bioactive nanoceramics. *International Journal of Molecular Sciences*, *17*(7), 1134. https://doi.org/10.3390/ijms17071134

Nájera-Romero, G. V., Yar, M., & Rehman, I. U. (2020). Heparinized chitosan/hydroxyapatite scaffolds stimulate angiogenesis. *Functional Composite Materials*, *1*(1), 9. https://doi.org/10.1186/s42252-020-00012-y

Park, K. H., Kim, S. J., Jeong, Y. H., Moon, H. J., Song, H. J., & Park, Y. J. (2018). Fabrication and biological properties of calcium phosphate/chitosan composite coating on titanium in modified SBF. *Materials Science and Engineering: C*, *90*(April), 113–118. https://doi.org/10.1016/j.msec.2018.04.060

Qasim, S. B. (2015). *Development of a novel bioactive functionally guided tissue graded membrane for periodontal lesions*. The University of Sheffield. https://doi.org/10.15445/01012014.07

Qasim, S. B., Delaine-Smith, R. M., Fey, T., Rawlinson, A., & Rehman, I. U. (2015). Freeze gelated porous membranes for periodontal tissue regeneration. *Acta Biomaterialia*, *23*, 317–328. https://doi.org/10.1016/j.actbio.2015.05.001

Qasim, S. B., Husain, S., Huang, Y., Pogorielov, M., Deineka, V., Lyndin, M., Rawlinson, A., & Rehman, I. U. (2017). In-vitro and in-vivo degradation studies of freeze gelated porous chitosan composite scaffolds for tissue engineering applications. *Polymer Degradation and Stability*, *136*, 31–38. https://doi.org/10.1016/j.polymdegradstab.2016.11.018

Ressler, A., Ródenas-Rochina, J., Ivanković, M., Ivanković, H., Rogina, A., & Gallego Ferrer, G. (2018). Injectable chitosan-hydroxyapatite hydrogels promote the osteogenic differentiation of mesenchymal stem cells. *Carbohydrate Polymers*, *197*(May), 469–477. https://doi.org/10.1016/j.carbpol.2018.06.029

Rogina, A., Ressler, A., Matić, I., Gallego Ferrer, G., Marijanović, I., Ivanković, M., & Ivanković, H. (2017). Cellular hydrogels based on pH-responsive chitosan-hydroxyapatite system. *Carbohydrate Polymers*, *166*, 173–182. https://doi.org/10.1016/j.carbpol.2017.02.105

Rokhade, A. P., Patil, S. A., & Aminabhavi, T. M. (2007). Synthesis and characterization of semi-interpenetrating polymer network microspheres of acrylamide grafted dextran and chitosan for controlled release of acyclovir. *Carbohydrate Polymers*, *67*(4), 605–613. https://doi.org/10.1016/j.carbpol.2006.07.001

Rouwkema, J., Boer, J. D., & Van Blitterswijk, C. A. (2006). Endothelial cells assemble into a 3-dimensional prevascular network in a bone tissue engineering construct. *Tissue Engineering*, *12*(9), 2685–2693. https://doi.org/10.1089/TEN.2006.12.2685

Sa, Y., Wang, M., Deng, H., Wang, Y., & Jiang, T. (2015). Beneficial effects of biomimetic nano-sized hydroxyapatite/antibiotic gentamicin enriched chitosan–glycerophosphate hydrogel on the performance of injectable polymethylmethacrylate. *RSC Advances*, *5*(110), 91082–91092. https://doi.org/10.1039/C5RA15915F

Shahzad, S., Yar, M., Siddiqi, S. A., Mahmood, N., Rauf, A., Qureshi, Z. A., Anwar, M. S., & Afzaal, S. (2015). Chitosan-based electrospun nanofibrous mats, hydrogels and cast films: Novel anti-bacterial wound dressing matrices. *Journal of Materials Science: Materials in Medicine*, *26*(3), 136. https://doi.org/10.1007/s10856-015-5462-y

Shahzadi, L., Chaudhry, A. A., Aleem, A. R., Malik, M. H., Ijaz, K., Akhtar, H., Alvi, F., Khan, A. F., Rehman, I. U., & Yar, M. (2018). Development of K-doped ZnO nanoparticles encapsulated crosslinked chitosan based new membranes to stimulate angiogenesis in tissue engineered skin grafts. *International Journal of Biological Macromolecules*, *120*, 721–728. https://doi.org/10.1016/j.ijbiomac.2018.08.103

Sharma, S., Sudhakara, P., Singh, J., Ilyas, R. A., Asyraf, M. R. M., & Razman, M. R. (2021). Critical review of biodegradable and bioactive polymer composites for bone tissue engineering and drug delivery applications. *Polymers*, *13*(16), 2623. https://doi.org/10.3390/polym13162623

Shive, M. S., Hoemann, C. D., Restrepo, A., Hurtig, M. B., Duval, N., Ranger, P., Stanish, W., & Buschmann, M. D. (2006). BST-CarGel: In situ chondroinduction for cartilage repair. *Operative Techniques in Orthopaedics*, *16*(4), 271–278. https://doi.org/10.1053/j.oto.2006.08.001

Sun, X., Peng, W., Yang, Z., Ren, M., Zhang, S., Zhang, W., Zhang, L., Xiao, K., Wang, Z., Zhang, B., & Wang, J. (2011). Heparin-chitosan-coated acellular bone matrix enhances perfusion of blood and vascularization in bone tissue engineering scaffolds. *Tissue Engineering. Part A*, *17*, 2369–2378. https://doi.org/10.1089/ten.tea.2011.0027

Taghizadeh, M., Taghizadeh, A., Yazdi, M. K., Zarrintaj, P., Stadler, F. J., Ramsey, J. D., Habibzadeh, S., Hosseini Rad, S., Naderi, G., Saeb, M. R., Mozafari, M., & Schubert, U. S. (2022). Chitosan-based inks for 3D printing and bioprinting. *Green Chemistry*, *24*(1), 62–101. https://doi.org/10.1039/d1gc01799c

Yancopoulos, G. D., Davis, S., Gale, N. W., Rudge, J. S., Wiegand, S. J., & Holash, J. (2000). Vascular-specific growth factors and blood vessel formation. *Nature*, *407*(Issue 6801), 242–248. https://doi.org/10.1038/35025215

Yang, H. S., La, W. G., Bhang, S. H., Jeon, J. Y., Lee, J. H., & Kim, B. S. (2010). Heparin-conjugated fibrin as an injectable system for sustained delivery of bone morphogenetic protein-2. *Tissue engineering. Part A*, *16*(4), 1225–1233. https://doi.org/10.1089/ten.tea.2009.0390

Yar, M., Gigliobianco, G., Shahzadi, L., Dew, L., Siddiqi, S. A., Khan, A. F., Chaudhry, A. A., Rehman, I., & MacNeil, S. (2016). Production of

chitosan PVA PCL hydrogels to bind heparin and induce angiogenesis. *International Journal of Polymeric Materials and Polymeric Biomaterials*, *65*(9), 466–476. https://doi.org/10.1080/00914037.2015.1129959

Yar, M., Shahzad, S., Shahzadi, L., Shahzad, S. A., Mahmood, N., Chaudhry, A. A., Rehman, I., & MacNeil, S. (2017). Heparin binding chitosan derivatives for production of pro-angiogenic hydrogels for promoting tissue healing. *Materials Science and Engineering: C*, *74*, 347–356. https://doi.org/10.1016/j.msec.2016.12.021

How to cite this article: Kocak, F. Z., Yar, M., & Rehman, I. U. (2024). In vitro degradation, swelling, and bioactivity performances of in situ forming injectable chitosan-matrixed hydrogels for bone regeneration and drug delivery. *Biotechnology and Bioengineering*, 1–13. https://doi.org/10.1002/bit.28755